Title: An Integrated Domain-Based Evolution Model for Red Sea: New Sea-Floor Spreading Evidence

Author information

Name: Farhoud, Khamis

Position: Study and Seismic Team Lead, Anton Oil, Majnoon Oil Field, Basra, Iraq

Email: kh_farhoud@hotmail.com

Phone No.: +201116055558

Name: El-Barkooky, Ahmed N.

Position: Professor in the Geology Department of Cairo University Email:

abarkook@cu.edu.eg

Status of this Manuscript: This is a non-peer-reviewed preprint submitted to EarthArXiv.

An Integrated, Domain-Based Evolution Model for the Red Sea: New Seafloor Spreading Evidence

Khamis Farhoud*, Ahmed N. El-Barkooky

*Corresponding author: kh_farhoud@hotmail.com

keywords: Red Sea, Seafloor Spreading, Magnetic Stripes, Structural Inheritance, Arabian-Nubian Shield

Abstract

The evolution and lateral extent of oceanic accretion within the central and northern Red Sea remain subjects of long-standing tectonic debate. Although the presence of young oceanic crust beneath the southern axial trough is widely accepted, uncertainty persists regarding whether complete separation between the Arabian and Nubian plates has occurred across the basin or whether oceanic crust remains restricted to the narrow Median Ridge Valley. In this study, the crustal architecture of the Red Sea is investigated through an integrated analysis of magnetic, gravity, bathymetric, seismic, and stratigraphic datasets. Organized magnetic anomaly patterns identified in the Central Red Sea suggest a prolonged phase of seafloor spreading lasting at least ~12.5 Ma. To evaluate this domain-based evolutionary framework independently of magnetic observations alone, regional two-dimensional gravity forward models, lithospheric density profiles, and deep multichannel seismic reflection and refraction datasets were incorporated. The integrated results indicate that the basement framework is strongly segmented by fault systems associated with the offshore continuation of Precambrian suture zones and the Dead Sea-Aqaba transform system, which influence the lateral offset and fragmentation of oceanic domains. Combined geophysical and stratigraphic evidence suggests the presence of a laterally continuous mafic crustal domain in the Central Red Sea extending up to ~125 km from the Median Ridge Valley. These observations imply that the ocean-continent boundary may lie close to the present-day coastlines and provide a revised tectonic framework for understanding the spatial and temporal evolution of Red Sea rifting.

1. Introduction

Considerable research has focused on the evolution of the Red Sea and the transition from continental rifting to seafloor spreading. Despite decades of investigation, fundamental questions remain regarding the nature and extent of oceanic crust, the location of the ocean-continent boundary, and the role of Proterozoic structures in controlling rift development. In particular, uncertainty persists as to whether complete separation between the Arabian and Nubian plates has occurred across the basin or whether oceanic crust remains restricted to the narrow Median Ridge Valley (MRV). To address these issues, the present study integrates magnetic, gravity, bathymetric, seismic, stratigraphic, and geological observations (Fig. 1a-e) to develop a domain-based model for Red Sea evolution.

Early investigations documented positive gravity anomalies along the Red Sea margins [1, 2] and recognized the axial trough as a system of narrow, linear depressions [3, 4]. Subsequent studies associated the axial region with basic intrusions and deep troughs (Fig. 1c and d) [5-7], while regional tectonic reconstructions linked these features to the relative motion between Arabia and Sinai [8-10]. Concurrently, regional surveys confirmed the existence of central deeps and identified reversely magnetized rocks in the Gulf of Aden [11, 12].

A major advance in understanding Red Sea evolution came with the recognition that magnetic lineations could be related to seafloor spreading processes [13]. Vine [14] simulated magnetic profiles for the Red Sea axial depression using a spreading rate of 1 cm/yr at latitudes 16° and 20°N. In parallel, seismic studies documented

crustal velocities between 6.7 and 7.3 km/s beneath the axial trough, accompanied by distinct gravity and magnetic signatures [15]. Subsequent investigations emphasized the importance of transform structures [16], refined the subdivision of the trough into axial and marginal zones [18], and suggested relatively young oceanic crust within the axial region [19, 20]. Magnetic studies at 19°N and 22°N inferred spreading ages of 2-4 Ma [21], while regional structural analyses related plate displacement to major shear zones [22]. Subsequent structural mapping delineated transform faults near 19°30'N [23, 24].

Even with these advances, the crustal configuration of the Red Sea remains controversial. Girdler [25] interpreted the basin as consisting predominantly of highly faulted continental crust (Fig. 1d), whereas McKenzie et al. [26] proposed that the entire Red Sea is underlain by oceanic crust. Other studies emphasized the influence of normal faulting [27], active volcanism [28], and MORB-type basalts recovered from Site 226 [29]. Interpretations based on the Miocene "S" seismic reflector suggested post-Miocene spreading [30], whereas alternative models proposed much older oceanic crust [31], younger magnetic anomalies [32], or oceanic domains extending into the northern Red Sea [33, 34].

Regional tectonic evolution is further complicated by the influence of the Danakil microplate [35], multiple phases of crustal development [36, 37], and contrasting interpretations derived from long regional gravity profiles [38]. Other studies recognized preserved continental blocks such as Zabargad Island [39] and subdivided the Red Sea into southern, central, and northern provinces [40]. Further investigations identified MORB-type basalts [41], proposed multi-stage tectonic evolution linked to the Aqaba-Dead Sea shear system [42], and described quasi-oceanic crust between 22°N and 25°N [43]. Debates concerning the extent and timing of oceanization have continued [44, 45], with spreading initiation estimates ranging from 10-12 Ma [46] to earlier proto-oceanic development beneath Miocene evaporites [47].

Increasing attention has been directed toward the role of tectonic inheritance in controlling Red Sea evolution. Oceanic-type seismic velocities have been reported as far north as 26°N [48, 49], while studies of Inter-Trough Zones and transverse structures attempted to reconcile competing crustal models [50-53]. Gravity analyses highlighted crustal thickening [54], and the Najd Shear System together with the Onib-Hamisana and Baraka sutures (Fig. 1e) were recognized as important structural controls [55]. The preservation of pre-rift formations [56], the largely amagmatic nature of the northern province [57, 58], and the influence of Afar-related magmatism [59, 60] further emphasize the complexity of Red Sea development. Lithospheric thinning at 15-12 Ma [61], south-to-north rift propagation [62], transtensional deformation [63], and oblique ridge geometries [64] have also been proposed. More recent studies have highlighted the importance of lithospheric inheritance, where the Arabian-Nubian Shield and major suture systems such as the Hamisana and Nakasib zones (Fig. 1e) act as fundamental templates for rift propagation [65, 66]. In addition, the masking effect of Miocene evaporites associated with the Messinian salinity crisis [67] may obscure older oceanic domains [68, 69]. Contemporary seismicity and volcanism along the Saudi Arabian margin provide further insight into ongoing lithospheric processes [70], while gravity-derived Euler reconstructions indicate marked latitudinal variations in crustal setting, with the central Red Sea containing mixed continental and oceanic domains and the northern sector remaining dominated by stretched continental lithosphere [71].

In view of these contrasting interpretations, the present study adopts an integrated geospatial approach combining magnetic, gravity, seismic, bathymetric, stratigraphic, and geological datasets. The objective is to evaluate the

spatial distribution of crustal domains, assess the influence of inherited Pan-African structures, and establish a unified framework for the temporal and structural evolution of the Red Sea.

2. Material and methods

To evaluate contrasting tectonic models of the Red Sea, this study employs a multi-proxy geospatial integration workflow combining gravity, magnetic, seismic, bathymetric, and stratigraphic datasets. These independent datasets were compiled within a unified georeferenced ArcGIS Pro framework to enable consistent spatial comparison and identification of crustal domains across the Red Sea basin.

2.1. Potential Field Analysis

Gravity and magnetic anomaly maps were analyzed to delineate the Median Ridge Valley (MRV) and to identify lateral offsets, linear anomalies, and anomaly terminations (Fig. 3e, f). Magnetic stripes were interpreted following the classical framework of Vine and Matthews [13], based on two principal characteristics:

1. Linearity of anomalies parallel to the spreading axis.
2. Organized alternation of magnetic polarity.

These features appear as elongated, strike-parallel bands of alternating positive and negative anomalies (dashed white lines, Fig. 3f). In contrast, isolated magmatic intrusions generally produce discrete, high-amplitude circular or irregular anomaly patterns with limited lateral continuity.

2.2. Rationale and Modeling Framework

This study adopts a domain-based framework that emphasizes anomaly continuity, symmetry, and termination. The analysis incorporates well established geomagnetic and gravity two-dimensional profiles [20, 21, 31, 38, 40, 46, 54]. These regenerated models (Fig. 4) provide well-established geophysical benchmarks based on the fundamental relationship between observed anomalies and source geometries. Previous studies indicate that magnetized blocks commonly occur between approximately 1.7 and 7.3 km below sea level, while gravity-derived density models identify a high-density basement extending across much of the Central Red Sea beneath an evaporite-rich sedimentary sequence with densities of approximately 2.2 g/cm^3.

By integrating these previously established constraints, the present analysis emphasizes the spatial relationships between geophysical observations and crustal domains rather than relying solely on parameter-dependent numerical fitting.

2.3. Seismic Velocity Compilation

The use of seismic velocities between 6.4 and 7.0 km/s as indicators of oceanic or intrusive crust is well established in Red Sea geophysics. In particular, the high-resolution datasets of Gaulier et al. (1988) documented velocities within this range beneath the evaporite sequence.

A composite seismic refraction profile approximately 1900 km long was reconstructed from VEMA-Atlantis datasets (Fig. 2). Crustal domains were classified according to seismic velocity [40, 46 and 48], with values exceeding 6.4 km/s interpreted as oceanic or intrusive crust and velocities below 6.4 km/s interpreted as continental crust. The resulting regional cross-section (Fig. 2) is displayed with a vertical exaggeration of 30:1 and a horizontal compression of approximately 7% relative to true scale to facilitate visualization.

2.4. Magnetic Spreading Correlation

A newly interpreted sequence of magnetic anomalies in the Central Red Sea (white dashed lines in Fig. 3f and Fig. 5b) was used to estimate the duration of seafloor spreading. Profile A-A' (Fig. 5b) has a true perpendicular width of approximately 125 km. Using a full spreading rate of approximately 1 cm yr^{-1} [14, 46], this width corresponds to a spreading duration of approximately 12.5 Ma. When considered together with the ~5 Ma age of the overlying Miocene S-reflector, these kinematic constraints suggest a total basement age of approximately 17.5 Ma for this part of the Central Red Sea.

The adopted spreading rate of 1 cm/yr is consistent with the slow-spreading characteristics proposed by Vine [14] and subsequently applied by Izzeldin [46] to the Red Sea. Although spreading rates may vary through time, significantly higher rates comparable to those observed at the Juan de Fuca Ridge or East Pacific Rise would imply crustal widths considerably greater than the present separation between the Arabian and Nubian shields. Consequently, the adopted rate provides a first-order kinematic framework that remains consistent with the regional geometry and plate displacement history.

To assess the consistency of this interpretation, the kinematic estimates were compared with independent geophysical observations (Fig. 4a-d). These include regional gravity models indicating the presence of relatively high-density mafic crust and seismic reflection and refraction datasets documenting basement continuity beneath the Miocene evaporite sequence (Fig. 2 and Fig. 4d). Collectively, these datasets provide a physically consistent framework supporting the interpretation of a prolonged spreading history extending beyond the present-day axial trough.

2.5. Bathymetric Analysis

Bathymetric data were analyzed to characterize axial trough morphology, basin segmentation, and depth variations along the Red Sea axis (Fig. 1c, d). These observations were evaluated together with gravity and magnetic datasets to assess the relationship between seafloor morphology and subsurface geophysical signatures.

2.6. Tectonic Inheritance

Onshore crystalline basement suture zones, including the Nakasib and Sol Hamid sutures (Fig. 1e), were georeferenced and projected offshore to evaluate their spatial relationship with geophysical anomalies and rift segmentation (Fig. 5a, b). This approach allows assessment of tectonic inheritance, whereby pre-existing crustal structures may influence the geometry of modern rifting.

2.7. Stratigraphic Integration

Chronological reference horizons were used to constrain the timing of the interpreted magnetic sequences (Fig. 3f). These include the Miocene regional marker (~5 Ma) and stratigraphic information from key exploration wells (Fig. 5b). The Jeddah-1 well encountered volcanic sequences within the Eocene interval [72], whereas the Durwara-2 well terminated in basalt at a depth of 4,152 m. In the Maghersum-1 well, the Mukwar Formation (Upper Cretaceous-Paleocene?) rests unconformably on basaltic basement [46], providing an additional stratigraphic constraint on the proposed model.

2.8. Geospatial Integration Framework

All datasets were integrated within a unified high-resolution georeferenced coordinate system using ArcGIS Pro. This framework ensures spatial consistency among geological, geophysical, bathymetric, and stratigraphic observations and enables systematic evaluation of spatial relationships independent of prior tectonic assumptions (Figs. 1 to 5).

3. Results

3.1. Characterization of Structural Provinces

Integration of georeferenced gravity, magnetic, bathymetric, seismic, and geological datasets delineates three distinct structural provinces and four dominant structural trends within the Red Sea basin.

- **Southern Province (15°30'N to 20°30'N)**
  This province is characterized by elongated and laterally continuous magnetic and gravity lineations extending for more than 800 km (Fig. 3e-f). These lineations coincide with a high-amplitude positive gravity anomaly approximately 110 km wide (Fig. 3e), centered on the Median Ridge Valley (MRV). Seismic refraction (Lines 170-178, Fig. 2) record crustal velocities exceeding 6.4 km/s, consistent with well-developed oceanic crust.
- **Central Province (20°30'N to 23°30'N)**
  The Central Province is characterized by organized magnetic polarity patterns (Fig. 3f, Fig.5b). North of the Heya terrane, magnetic anomalies become increasingly decoupled from gravity signatures, where the corresponding gravity anomalies decrease northward across the Nakasib-Heya-Jeddah terrane boundary (Fig. 5a). Seismic refraction velocities beneath the MRV remain relatively high (6.76-6.97 km/s; Lines 179-181, Fig. 2), while multichannel seismic reflection (location shown in Fig. 4e) indicate lateral continuity of high-velocity basement extending tens of kilometers away from the axis (Fig. 4d).
- **Northern Province (23°30'N to 27°30'N)**
  Pre-rift stratigraphic units, including the Zabargad Formation, are preserved within this province. Regions adjacent to the coastal margins (Fig. 2) exhibit geophysical characteristics compatible with continental basement, supported by seismic refraction velocities below 6.4 km/s. In contrast to the higher-velocity domains identified basinward, magnetic anomalies are generally weak and discontinuous and lack laterally continuous lineations. Overall, this province displays characteristics typical of an amagmatic continental rift (Fig. 5a-b).

3.2. Identification of Magnetic Stripes and Structural Offsets

Geospatial analysis identifies five groups of linear magnetic anomalies within the Central and Southern provinces (Fig. 3f). These anomalies are characterized by strike-parallel continuity and lengths ranging from approximately 100 to 220 km (Groups 1-4). Group 5 is comparatively more fragmented, with lineations segmented by small-scale strike-slip structures. The geometry and continuity of these anomalies are consistent with organized spreading-related patterns rather than isolated continental intrusions.

The identified stripe groups are offset by interpreted strike-slip structures (Fig. 3f), suggesting that basement fabrics and transform tectonics have influenced the segmentation of the oceanic domains.

A major structural discontinuity occurs near Atlantis II Deep at approximately 20°30'N, corresponding to the offshore projection of the Baraka Suture Zone (Fig. 3e and f; Fig. 5b and c). At this location, the gravity anomaly terminates abruptly (Fig. 3e and f), while the magnetic anomaly axis exhibits a lateral offset of approximately 64 km between the northern Group 1 and southern Group 2 domains (Fig. 3f and Fig. 5a). This displacement spatially coincides with the projected Baraka left-lateral suture and the Atlantis II transform fault (Fig. 3e), indicating that basement structures may have influenced the fragmentation and offset of the developing oceanic domains.

3.3. Spatial and Latitudinal Variations in Magnetic Fabric and Stripe Geometry

Analysis of the magnetic fabric reveals marked latitudinal variations in anomaly character among the five identified groups (Fig. 3f). Groups 1 and 2 in the northern sector are characterized by relatively high-amplitude positive anomalies with a prominent magenta axis associated with localized spreading centers.

Toward the south, Groups 3, 4, and 5 display a transition to predominantly negative or subdued magnetic signatures. In addition, the continuity of the linear anomaly patterns becomes increasingly disrupted by strike-slip offsets associated with transform faults and Precambrian structures, including the Nakasib suture zones (Figs. 3a-f).

These variations indicate significant along-axis changes in magnetic fabric and suggest differences in the structural style and evolution of the Red Sea spreading system.

3.4. Stratigraphic Constraints and Magnetic Correlation

Seismic refraction data at the eastern end of profile A-A' (Lines 180-181; Fig. 2 and Fig. 5a, b) record deep crustal velocities reaching 6.97 km/s. These values correspond spatially with seismic layer identified in previous studies (Fig. 4d). Multichannel seismic reflection lines (Fig. 4d and e) indicate lateral continuity of this high-velocity basement for approximately 80 km on either side of the axis.

Stratigraphic information from regional wells (Fig. 5b) provides extra constraints on basement characteristics. Subsurface control confirms this older mafic framework.

The interpreted magnetic anomalies (dashed white lines, Fig. 5b) define a sequence of organized polarity reversals extending approximately 250 km across the basin beneath the top Miocene. Accounting for a full spreading rate of 1 cm/yr, the 125 km sub-basin geometry signifies an accretionary window of roughly 12.5 Ma, pushing the initiation of central rifting back to the early Miocene (~17.5 Ma) when calibrated against the overlying evaporite marker.

Collectively, the magnetic, seismic, and stratigraphic observations indicate a pre-Pliocene framework for crustal accretion and basement development within the Central Red Sea.

3.5. Dominant Structural Trends

Four principal structural trends were identified through comparison of anomaly geometries with established regional tectonic fabrics (Fig. 3):

1. **N-S basement lineaments (Fig. 3a):** linear gravity and magnetic gradients associated with deep-seated fault systems.

2. **Suture trends (Fig. 3b):** offshore continuation of onshore terrane boundaries, including the Nakasib suture, marked by abrupt gravity terminations.
3. **NW-SE Najd shear fabrics (Fig. 3c):** Proterozoic structural fabrics within the Arabian-Nubian Shield.
4. **NE-SW strike-slip lineaments (Fig. 3d):** structures related to the Aqaba-Dead Sea transform system that locally offset magnetic anomalies. The Mabahiss Deep and Atlantis II transform faults represent prominent examples of this structural trend.

4. Discussion

The interpretation of Red Sea evolution presented in this study is based on an integrated spatial framework that emphasizes potential-field anomaly continuity, structural terminations, and cross-rift symmetry. This approach incorporates previously published two-dimensional gravity and magnetic models (Fig. 4), which provide established geophysical constraints for evaluating the spatial distribution of crustal domains. By combining these independent datasets (Figs. 4a-d) with the anomaly patterns identified in this study (Figs. 3 and 5), a regional framework is developed for assessing the spatial, temporal, and structural evolution of the Red Sea basin. Rather than relying solely on parameter-dependent numerical solutions, the analysis emphasizes the consistency between multiple geophysical and geological observations.

4.1. The Southern Red Sea Province

The southern Red Sea axial ridge is characterized by distinct, straight-sided bathymetric troughs that define the active rift zone (Fig. 1d). Although earlier models proposed widespread oceanization extending across the basin and dating back to approximately 40 Ma [31], such interpretations are difficult to reconcile with regional stratigraphic relationships, which indicate the preservation of older sedimentary successions along the margins. In contrast, the integrated potential-field datasets presented here suggest that the thickest and densest magmatic crustal material is largely concentrated within the Median Ridge Valley (MRV), forming a continuous structural belt approximately 110 km wide (Fig. 3e).

This oceanic domain extends northward along the principal rift axis and appears to terminate near 20°30′N, close to the offshore projections of the Baraka and Nakasib suture zones (Fig. 3e). The geometry of the gravity and magnetic anomalies further indicates that active crustal accretion in the southern province is influenced by NE-SW strike-slip faulting. These transform-related structures segment and laterally offset Groups 3, 4, and 5 (Fig. 3f), suggesting that pre-existing lithospheric structures exert an important control on the geometry and segmentation of the modern spreading system.

4.2. The Central Red Sea: Evidence for a Prolonged 12.5 Ma Spreading History

In the Central Red Sea province, the integrated geophysical observations support a domain-based evolutionary framework involving an early phase of oceanic accretion. The presence of organized linear magnetic anomalies (Group 1; Fig. 3f), which are overlain by the regional Miocene reflector (Fig. 4d), suggests that this crustal accretion predates deposition of the evaporite sequence. The inferred early initiation age (~17.5 Ma) suggests that crustal accretion in the central province may have begun earlier and extended farther laterally than models restricting oceanization to the young 2-3 Ma axial cells (Fig.5b and e). To evaluate the influence of the assumed spreading rate on the estimated duration of crustal accretion, a simple sensitivity analysis was performed using plausible full spreading rates around the adopted value of 1 cm/yr. Varying the full spreading rate from 0.8 to 1.2

cm/yr yields corresponding spreading durations of approximately 15.6 Ma and 10.4 Ma, respectively, compared with 12.5 Ma for the preferred rate of 1 cm/yr.

Although the estimated duration varies with the assumed spreading rate, the overall interpretation remains unchanged. In all cases, the inferred spreading history substantially predates the ~5 Ma top Miocene and supports the existence of an older phase of crustal accretion within the Central Red Sea. Consequently, the proposed domain-based framework is not dependent on a single kinematic solution but remains consistent across a reasonable range of spreading rates.

This interpretation is consistent with the observations of Izzeldin [46] and Gaulier et al. [48], who documented crustal velocities of 6.5-6.9 km/s across regionally persistent acoustic basement (Fig. 4d and Fig.2). Regional seismic reflection (Lines 1 to 27, Fig. 4e) further indicate the lateral continuity of this basement package, suggesting that the oceanic or mafic crustal domain extends toward the shore lines. Similarly, early refraction surveys (Fig.2) identified laterally continuous layers with velocities ranging from 6.6 to 7.3 km/s [20], values commonly associated with oceanic Layer 3 or mafic intrusive crust. When integrated with the regional gravity profiles of Brown and Girdler [38], which extend for more than 1,500 km across the basin (Fig. 4b), a broad positive Bouguer anomaly exceeding +100 mGal is observed. Reproducing this anomaly requires relatively dense crustal material with densities between 2.90 and 3.0 g/cm³, replacing surrounding continental lithosphere characterized by densities of 2.67 to 2.80 g/cm³. Notably, the approximately 250 km basin-wide extent of the interpreted magnetic domains (dashed white lines, Fig. 5b) spatially corresponds to the zone of maximum crustal densification.

The lithospheric framework (Figs. 4a-c) reveals progressive thinning toward the rift axis. Whereas the unrifted Afro-Arabian Shield preserves a typical three-layer continental crust (density ~2.85 g/cm³) overlying mantle material with densities near 3.35 g/cm³, the Moho beneath the Central Red Sea rises to depths of approximately 11 km (Figs. 4a-c). This attenuated crustal package includes material with densities approaching 2.88 g/cm³ beneath thick Miocene and Plio-Pleistocene sedimentary sequences that commonly exceed 4 km in thickness. The evaporitic sequence [46] may have obscured evidence of earlier spreading phases by masking much of the underlying basement geometry. Nevertheless, multichannel seismic reflection data reveal laterally continuous acoustic basement suggesting that the mafic crustal domain extends continuously toward the shores beneath the salt cover (Fig. 4d). Taken together, the density models, seismic observations, and geometric relationships are consistent with the presence of a laterally extensive mafic crustal domain and suggest that the ocean-continent boundary may lie considerably closer to the continental shelves than proposed in models restricting oceanization to the present axial trough.

The geometry and symmetry of the magnetic anomalies favor an interpretation involving sustained and organized spreading rather than localized volcanic centers. The magnetic maps (Fig. 3f) and profile A-A' (Fig. 5b) show a central positive anomaly flanked by repeated sequences of alternating negative and positive anomalies. This broadly symmetrical pattern extends across the basin and resembles the anomaly geometry expected from prolonged seafloor spreading. Correlation with the geomagnetic polarity timescale (GSA, 2022; Fig. 5e) indicates a possible correspondence with chrons C20-C24. However, magnetostratigraphic correlations are inherently non-unique and should therefore be regarded as tentative.

Independent stratigraphic constraints from exploration wells provide support for an older basement age (Fig. 5b). Lithostratigraphic evidence from exploratory wells further constrains this timing, noting pre-Miocene sequences across the Maghersum, Durwara, and Jeddah [46], indicating that the basement underlying the Central Red Sea predates the Pliocene. The character of the magnetic signal itself provides further support, as profile A-A' (Fig. 5e) displays long-wavelength, low-frequency polarity transitions that differ from the higher-frequency anomalies commonly associated with younger and narrower active spreading segments.

The systematic polarity and amplitude differences observed between the northern and southern magnetic groups (Fig. 3f) further suggest along-axis variations in spreading style and tectonic evolution. Groups 1 and 2 are characterized by relatively strong positive anomalies, whereas Groups 3, 4, and 5 exhibit weaker and more fragmented signatures. These variations may reflect differences in spreading history, fault segmentation, or subsequent tectonic modification associated with inherited structures and transform faulting. In particular, the strong structural segmentation affecting the southern Red Sea may contribute to suppression of magnetic amplitudes regardless of the presence of active magmatism.

4.3. The Northern Red Sea Province

In contrast to the more pronounced magmatic signatures observed in the central and southern sectors, the northern Red Sea exhibits characteristics consistent with an amagmatic continental rift. The preservation of pre-rift stratigraphy at Zabargad Island (see Fig. 5b for location), together with deep seismic refraction velocities below 6.4 km/s near the continental margins (Fig. 2), is compatible with a stretched continental basement. Correspondingly, magnetic and gravity anomalies north of the Sol Hamed-Allaqi Suture Zone (Fig.3e and Fig. 5b) are generally weak, low-amplitude, and laterally discontinuous. These potential-field characteristics are consistent with diffuse lithospheric extension and block faulting rather than the more organized seafloor spreading inferred for the central and southern Red Sea provinces.

4.4. Structural Control: Suture Zones and Tectonic Inheritance

The distribution of the structural provinces identified in this study appears to be closely associated with major suture zones, which influence the lateral extent and segmentation of magmatic accretion. The Nakasib and Baraka Suture Zones form an important southern boundary separating the active spreading system of the southern province from the older oceanic domain inferred in the central province (Fig. 3e and f).

In addition, the approximately 64 km lateral offset observed along the central Red Sea rift axis (black arrow, Fig. 5a) spatially coincides with the onshore Baraka suture and its offshore continuation along the Atlantis II transform fault (Fig. 3d, e and f). This correspondence suggests that old shear structures may have acted as important lithospheric templates influencing the geometry, segmentation, and lateral displacement of the developing rift system (Fig. 5a and c).

Conversely, the Sol Hamed-Allaqi Suture Zone (Figs. 3b, f and 5a) appears to mark the northern limit of organized oceanization. Near this terrane boundary, the coherent strike-parallel magnetic lineations observed in the central province gradually transition into the weaker and more discontinuous anomaly patterns characteristic of the northern Red Sea (Fig. 5b). From a potential-field perspective, these suture zones appear to represent major lithospheric boundaries separating domains characterized by organized spreading from regions dominated by old continental structures.

Synthesizing these regional observations, the integrated geological and geophysical datasets suggest that Red Sea evolution has been strongly influenced by the structural geometry of the Arabian-Nubian Shield (Fig. 3a-d). Within this framework, three principal evolutionary domains can be recognized (Fig. 5c):

1. **Southern Province (Fig. 3e and f):** axial-restricted oceanic spreading influenced by transform-related segmentation.
2. **Central Province (Fig. 3f and Fig. 5b):** an older oceanic domain representing a prolonged phase of early spreading, with a minimum basement age of approximately 17.5 Ma preserved beneath the Miocene evaporite sequence.
3. **Northern Province**: diffuse amagmatic continental rifting influenced by Neoproterozoic basement fabrics and overprinted by NE-SW strike-slip deformation associated with the Dead Sea-Aqaba transform system.

4.5. Hydrocarbon Exploration Significance of the Proposed Red Sea Evolution Model

1. From an exploration perspective, the distribution of modern oceanization cells and volcanic centers (Fig.1c and Fig.5a) introduces a significant thermal and structural risk along the axial trough and the Median Ridge Valley. These zones correspond to active or relatively young magmatic domains, crustal thinning, transform faulting, and hydrothermal activity. Such conditions are generally unfavorable for conventional hydrocarbon accumulations. In addition, the presence of young mafic crust reduces the accommodation space for thick pre-rift sedimentary successions and increases the likelihood of volcanic intrusions, uplift, and local thermal over maturation. Consequently, the immediate vicinity of the modern spreading axis and hot-spot-related oceanization cells should be regarded as a high-risk exploration domain, despite the possibility of localized structural closures associated with transform faults and pull-apart basins.
2. In contrast, the domain-based framework proposed here suggests that the most prospective petroleum systems are likely to occur away from the active axial zone, particularly within the Central and Northern provinces where pre-existing structures control basin configuration. If the ocean-continent boundary lies near the coast, as indicated by the integrated geophysical observations, **then the continental margins and transitional domains adjacent to the Nakasib and Sol Hamed-Allaqi suture zones become favorable targets for preserving thick pre-rift successions.** The Jeddah-1, Durwara-2, and Maghersum-1 wells indicate that volcanic or mafic basement may be overlain by Paleocene, Upper Cretaceous, and younger sedimentary sequences, implying that older source intervals could remain preserved outside the axial oceanization cells. Structural styles in these domains are expected to be dominated by rotated fault blocks, horst-graben systems, tilted basement highs, inversion structures, and salt-related traps beneath the Miocene evaporites. Therefore, the proposed three-domain model (Fig. 5c) implies a clear exploration strategy: the highest geological risk is concentrated along the active axial spreading centers, whereas the greatest potential for conventional hydrocarbon accumulations resides within the marginal and transitional sectors of the Central and Northern

Red Sea (Sol Hamid), where older sedimentary packages are more likely to have survived and where structural and stratigraphic trapping mechanisms are expected to be most effective.

4.6. Alternative Explanations for the Central Red Sea Magnetic Anomalies

Magnetic interpretations are inherently non-unique, and alternative explanations for the anomaly patterns observed in the Central Red Sea, including isolated intrusions and volcanic centers, must therefore be considered. However, several characteristics favor an interpretation involving organized crustal accretion.

The anomalies exhibit elongated strike-parallel geometries, repeated polarity alternations, and systematic segmentation that spatially coincide with transform faults and offshore projections of major suture zones (Figs. 3f and 5a). Such regionally coherent patterns are difficult to reconcile with isolated volcanic centers or localized basement highs and instead suggest tectonic control associated with organized crustal development.

Independent geophysical observations provide additional support for this interpretation. Seismic refraction studies document velocities exceeding 6.4 km/s [20, 46, 48], while multichannel seismic reflection data indicate laterally continuous basement beneath the Miocene evaporite sequence (Fig. 4d). Likewise, three independent gravity models developed over nearly five decades (Fig. 4a-c) consistently indicate a broad high-density central domain (≈2.9-3.0 g/cm³) associated with crustal thinning, Moho uplift, and long-wavelength positive gravity anomalies. Together, these features imply the presence of laterally extensive mafic crust extending well beyond the present Median Ridge Valley.

Although alternative explanations cannot be entirely excluded, the convergence of magnetic, gravity, seismic, and stratigraphic observations favors an interpretation involving prolonged and organized crustal accretion in the Central Red Sea. The resulting crustal framework is therefore more consistent with a first-order lithospheric feature than with isolated magmatic centers and suggests that Red Sea evolution has been strongly influenced by the inherited structural framework of the Arabian-Nubian Shield. Future high-resolution marine magnetic surveys and targeted deep seismic investigations may further constrain the symmetry and timing of this early phase of spreading.

Conclusion

This study presents a unified, multi-proxy, domain-based framework for investigating the crustal evolution of the Red Sea. By integrating georeferenced potential-field datasets, regional seismic refraction lines, multichannel seismic reflection, and well constraints within a common geospatial framework, three structurally distinct provinces are identified whose lateral boundaries appear to be strongly influenced by the pre-existing architecture of the Arabian-Nubian Shield.

The results indicate that active modern seafloor spreading in the Southern Province is largely confined to a zone approximately 110 km wide within the axial trough and appears to terminate near 20°30'N, close to the offshore projection of the Baraka Suture Zone. In contrast, the Central Province contains evidence for a laterally extensive mafic basement domain extending up to approximately 125 km from the axis. Kinematic constraints and organized magnetic anomalies preserved beneath the regional Miocene horizon are consistent with a prolonged phase of paleo-spreading that operated for approximately 12.5 Ma during the early evolution of the basin. Conversely, the Northern Province, bounded to the south by the Sol Hamed-Allaqi Suture Zone, exhibits characteristics consistent

with an amagmatic continental rift, including diffuse extension, weak potential-field anomalies, and seismic velocities compatible with continental basement.

Overall, these observations suggest that the Red Sea evolved as a laterally variable and strongly segmented rift system rather than as a uniform and continuous spreading center. The timing, geometry, and extent of magmatic accretion appear to have been significantly influenced by Neoproterozoic structures and by transform-related deformation, which together contributed to the segmentation and lateral offset of crustal domains.

References

1. Von Triulzi, A. E. *Denkschr. Akad. Wiss. Wien Math.-Nat. Kl.* **65**, 131 (1898).
2. Vening Meinesz, F. A. *Gravity Expeditions at Sea, 1923–1932*, Vol. II. (Netherlands Geodetic Commission, Delft, 1934). https://doi.org/10.54419/3us2nj
3. Farquharson, W. I. Topography, with an appendix on magnetic observations. *Sci. Rep. John Murray Exped. 1933-34* **1**, 43–61 (1935).
4. Owen, L. Origin of the Red Sea depression. *AAPG Bull.* **22**, 1217–1223 (1938). https://doi.org/10.1306/3d932fe0-16b1-11d7-8645000102c1865d
5. Girdler, R. W. The relationship of the Red Sea to the East African Rift System. *Q. J. Geol. Soc. Lond.* **114**, 79–105 (1958). https://doi.org/10.1144/gsjgs.114.1.0079
6. Tazieff, H. Une recente campagne oceanographique dans la mer Rouge. *Bull. Soc. Belge Geol.* **61**, 84–90 (1952).
7. Girdler, R. W. & Harrison, J. C. Submarine gravity measurements in the Atlantic, Indian Ocean, Red Sea and Mediterranean Sea. *Proc. R. Soc. Lond. A* **239**, 202 (1957). https://doi.org/10.1098/rspa.1957.0033
8. Quennell, A. M. Tectonics of the Dead Sea rift. in *Proc. 20th Int. Geol. Congr.* 385–405 (Mexico City, 1956).
9. Quennell, A. M. Tectonics of the Dead Sea rift. *Assoc. Afr. Geol. Surv.* 385–408 (1959).
10. Carey, S. W. A tectonic approach to continental drift. in *Continental Drift: A Symposium* 177–355 (University of Tasmania, Hobart, 1958).
11. Drake, C. L., Girdler, R. W. & Landisman, M. Geophysical measurements in the Red Sea. in *Proc. Int. Oceanogr. Congr.* 20 (New York, 1959).
12. Girdler, R. W. & Peter, G. An example of the importance of natural remanent magnetization in the interpretation of magnetic anomalies. *Geophys. Prospect.* **8**, 474–483 (1960). https://doi.org/10.1111/j.1365-2478.1960.tb01730.x
13. Vine, F. J. & Matthews, D. H. Magnetic anomalies over ocean ridges. *Nature* **199**, 947–949 (1963). https://doi.org/10.1038/199947a0
14. Vine, F. J. Spreading of the ocean floor: New evidence. *Science* **154**, 1405–1415 (1966). https://doi.org/10.1126/science.154.3755.1405
15. Drake, C. L. & Girdler, R. W. A geophysical study of the Red Sea. *Geophys. J.* **8**, 473–495 (1964). https://doi.org/10.1111/j.1365-246X.1964.tb06303.x
16. Wilson, J. T. Transform faults, oceanic ridges and magnetic anomalies southwest of Vancouver Island. *Science* **150**, 482–485 (1965). https://doi.org/10.1126/science.150.3695.482
17. Allan, T. D. A bathymetric chart of the Red Sea. *Int. Hydrogr. Rev.* **43**, 33–36 (1966).
18. Knott, S. T., Bunce, E. T. & Chase, R. L. Red Sea seismic reflection studies. *Geol. Surv. Can. Pap.* **66-14**, 33–61 (1966). https://doi.org/10.4095/103358
19. Girdler, R. W. Earth satellites, terrestrial heat flow, mantle convection and the location of extensional and compressional features on the Earth's surface. *Proc. Geol. Assoc.* **78**, 165–178 (1967). https://doi.org/10.1016/s0016-7878(67)80042-7

20. Tramontini, C. & Davies, D. Seismic refraction survey in the Red Sea. *Geophys. J.* **17**, 225–241 (1969). https://doi.org/10.1111/j.1365-246x.1969.tb02323.x

21. Phillips, J. D., Woodside, J. & Bowin, C. O. Magnetic and gravity anomalies in the central Red Sea. in *Hot Brines and Recent Heavy Metal Deposits in the Red Sea* (eds Degens, E. T. & Ross, D. A.) 98–113 (Springer, Berlin, 1969). https://doi.org/10.1007/978-3-662-28603-6_10

22. Abdel-Gawad, M. Geological structures of the Red Sea area inferred from satellite pictures. in *Hot Brines and Recent Heavy Metal Deposits in the Red Sea* (eds Degens, E. T. & Ross, D. A.) 25–37 (Springer, Berlin, 1969). https://doi.org/10.1007/978-3-662-28603-6_5

23. Phillips, J. & Ross, D. A. Continuous seismic reflection profiles in the Red Sea. *Philos. Trans. R. Soc. Lond. A* **267**, 143–152 (1970). https://doi.org/10.1098/RSTA.1970.0029

24. Allan, T. D. Magnetic and gravity fields over the Red Sea. *Philos. Trans. R. Soc. Lond. A* **261**, 153–180 (1970). https://doi.org/10.1098/rsta.1970.0030

25. Girdler, R. W. A review of Red Sea heat flow. *Philos. Trans. R. Soc. Lond. A* **267**, 359–368 (1970). https://doi.org/10.1098/rsta.1970.0032

26. McKenzie, D. P., Davies, D. & Molnar, P. Plate tectonics of the Red Sea and East Africa. *Nature* **226**, 243–248 (1970). https://doi.org/10.1038/226243a0

27. Lowell, J. D. & Genik, G. J. Sea-floor spreading and structural evolution of the southern Red Sea. *AAPG Bull.* **56**, 247–259 (1972). https://doi.org/10.1306/819a3e56-16c5-11d7-8645000102c1865d

28. Stieltjes, L. Evolution tectonique recente du rift d'Asal. *Rev. Geogr. Phys. Geol. Dyn.* **15**, 425–436 (1973).

29. Stoffers, P. & Ross, D. A. Sedimentary history of the Red Sea. *Initial Rep. Deep Sea Drill. Proj.* **23**, 849–865 (1974). https://doi.org/10.2973/dsdp.proc.23.123.1974

30. Roger, C., Searle, R. & Ross, D. A. Geophysical study of the Red Sea axial trough. *Geophys. J. R. Astron. Soc.* **43**, 555–572 (1975). https://doi.org/10.1111/j.1365-246x.1975.tb00647.x

31. Girdler, R. W. & Styles, P. Two-stage Red Sea floor spreading. *Nature* **247**, 7–11 (1974). https://doi.org/10.1038/247007a0

32. Roeser, H. A. Detailed magnetic survey of the southern Red Sea. *Geol. Jahrb.* **13**, 131–153 (1975).

33. Gettings, M. E. Delineation of the continental margin of the southern Red Sea from new gravity evidence. *Saudi Arab. Dir. Gen. Miner. Res. Bull.* **2**, K1–K11 (1977).

34. Girdler, R. W. & Southren, T. Structure and evolution of the northern Red Sea. *Nature* **330**, 716–721 (1987). https://doi.org/10.1038/330716a0

35. Le Pichon, X. & Francheteau, J. Plate tectonic analysis of the Red Sea–Gulf of Aden area. *Tectonophysics* **46**, 369–406 (1978). https://doi.org/10.1016/0040-1951(78)90214-7

36. Girdler, R. W., Brown, C., Noy, D. J. M. & Styles, P. Geophysical survey of the westernmost Gulf of Aden. *Philos. Trans. R. Soc. Lond. A* **298**, 1–43 (1980). https://doi.org/10.1098/rsta.1980.0239

37. LaBrecque, J., Kent, D. V. & Cande, S. C. Revised magnetic polarity time scale for Late Cretaceous and Cenozoic time. *Geology* **5**, 330–335 (1977). https://doi.org/10.1130/0091-7613(1977)5-330-RMPTSF-2.0.CO-2

38. Brown, C. & Girdler, R. W. Structure of the Red Sea at 20° N from gravity data and its implications for continental margins. *Nature* **298**, 51–53 (1982). https://doi.org/10.1038/298051a0

39. Courtillot, V. Propagating rifts and continental breakup. *Tectonics* **1**, 239–250 (1982). https://doi.org/10.1029/TC001i003p00239

40. Cochran, J. R. A model for development of Red Sea. *AAPG Bull.* **67**, 41–69 (1983). https://doi.org/10.1306/03B5ACBE-16D1-11D7-8645000102C1865D

41. Bonatti, E., Colantoni, P., Della Vedova, B. & Taviani, M. Geology of the Red Sea transitional region (22° N–25° N). *Oceanol. Acta* **7**, 385–398 (1984).

42. Girdler, R. W. Problems concerning the evolution of oceanic lithosphere in the northern Red Sea. *Tectonophysics* **116**, 109–122 (1985). https://doi.org/10.1016/0040-1951(85)90224-0

514 43. LaBrecque, J. L. & Zitellini, N. Continuous seafloor spreading in the Red Sea. *AAPG Bull.* **69**, 513–524
515 (1985). https://doi.org/10.1306/AD46251F-16F7-11D7-8645000102C1865D

516 44. Bicknell, J. D. et al. Tectonics of the Nereus Deep, Red Sea: A deep-tow investigation of a site of initial
517 rifting. *J. Geophys. Res.* **91**, 4801–4810 (1986). https://doi.org/10.1007/bf00338225

518 45. Bonatti, E. Rifting or drifting in the Red Sea? *Nature* **330**, 692–693 (1987).
519 https://doi.org/10.1038/330692a0

520 46. Izzeldin, A. Y. Seismic, gravity and magnetic surveys in the central part of the Red Sea. *Tectonophysics*
521 **143**, 269–306 (1987). https://doi.org/10.1016/0040-1951(87)90214-9

522 47. Joffe, S. & Garfunkel, Z. Plate kinematics of the circum–Red Sea: A re-evaluation. *Tectonophysics* **141**,
523 5–23 (1987). https://doi.org/10.1016/0040-1951(87)90171-5

524 48. Gaulier, J. M. et al. Seismic study of the crust of the northern Red Sea and Gulf of Suez. *Tectonophysics*
525 **153**, 55–88 (1988). https://doi.org/10.1016/0040-1951(88)90007-8

526 49. Martinez, F. & Cochran, J. R. Structure and tectonics of the northern Red Sea. *Tectonophysics* **150**, 1–
527 32 (1988). https://doi.org/10.1016/0040-1951(88)90293-4

528 50. Izzeldin, A. Y. Transverse structures in the central Red Sea and implications for early oceanic accretion.
529 *Geophys. J.* **96**, 117–129 (1989). https://doi.org/10.1111/j.1365-246X.1989.tb05254.x

530 51. Guennoc, P., Pautot, G., Le Quentrec, M.-F. & Coutelle, A. Structure of an early oceanic rift in the
531 northern Red Sea. *Oceanol. Acta* **13**, 145–155 (1990).

532 52. Uchupi, E. & Ross, D. A. The geologic enigma of the Red Sea rift. in *Facets of Modern Biogeochemistry*
533 (eds Ittekkot, V. et al.) 52–61 (Springer, Berlin, 1990).

534 53. Girdler, R. W. The case for oceanic crust beneath the Red Sea. *Tectonophysics* **198**, 275–278 (1991).
535 https://doi.org/10.1016/0040-1951(91)90155-L

536 54. Makris, J. & Rihm, R. Shear-controlled evolution of the Red Sea. *Tectonophysics* **198**, 441–466 (1991).
537 https://doi.org/10.1016/0040-1951(91)90166-p

538 55. Makris, J. & Henke, C. H. Pull-apart evolution of the Red Sea. *J. Pet. Geol.* **15**, 127–134 (1992).
539 https://doi.org/10.1111/j.1747-5457.1992.tb00958.x

540 56. Bosworth, W. et al. Stratigraphic and structural evolution of Zabargad Island (Red Sea, Egypt) since the
541 Early Cretaceous. in *Proc. 3rd Int. Conf. Geol. Arab World* (ed. El-Ayouty, M.) 161–190 (Cairo
542 University, 1996).

543 57. Bosworth, W. & McClay, K. R. Structural and stratigraphic evolution of the Gulf of Suez Rift, Egypt. in
544 *Peri-Tethys Memoir 6: Peritethyan Rift/Wrench Basins and Passive Margins* (eds Ziegler, P. A. et al.)
545 567–606 (Muséum national d'Histoire naturelle, Paris, 2001).

546 58. Cochran, J. R. Northern Red Sea: Nucleation of an oceanic spreading center within a continental rift.
547 *Geochem. Geophys. Geosyst.* **6**, Q03006 (2005). https://doi.org/10.1029/2004gc000826

548 59. Bosworth, W. Geological evolution of the Red Sea: Historical background, review, and synthesis. in *The*
549 *Red Sea* (eds Rasul, N. M. A. & Stewart, I. C. F.) 45–78 (Springer Earth System Sciences, Berlin, 2015).
550 https://doi.org/10.1007/978-3-662-45201-1_3

551 60. Bosworth, W. & Stockli, D. F. Early magmatism in the greater Red Sea. *Can. J. Earth Sci.* **53**, 1158–
552 1176 (2016). https://doi.org/10.1139/cjes-2016-0019

553 61. Blanchette, A. R., Klemperer, S. L., Mooney, W. D. & Zahran, H. M. Two-stage Red Sea rifting inferred
554 from mantle earthquakes in Neoproterozoic lithosphere. *Earth Planet. Sci. Lett.* **497**, 92–101 (2018).
555 https://doi.org/10.1016/j.epsl.2018.05.048

556 62. Bosworth, W., Khalil, S. M., Ligi, M., Stockli, D. F. & McClay, K. R. The northern Red Sea. in *The*
557 *Geology of Egypt* (eds Hamimi, Z. et al.) 344–369 (Springer, Cham, 2020). https://doi.org/10.1007/978-
558 3-030-15265-9_9

559 63. Issachar, R., Ebbing, J. & Dilixiati, Y. New magnetic anomaly map for the Red Sea reveals transtensional
560 structures associated with rotational rifting. *Sci. Rep.* **12**, 5757 (2022). https://doi.org/10.1038/s41598-
561 022-09770-0

562 64. Delaunay, A. et al. Structure and morphology of the Red Sea, from the mid-ocean ridge to the ocean-
563 continent boundary. Tectonophysics 849, 229728 (2023). https://doi.org/10.1016/j.tecto.2023.229728

65. Issachar, R., Haas, P., Augustin, N. & Ebbing, J. Rift and plume: a discussion on active and passive rifting mechanisms in the Afro-Arabian rift based on synthesis of geophysical data. *Solid Earth* **15**, 807–826 (2024). https://doi.org/10.5194/se-15-807-2024

66. Phillips, T. B. *et al.* The influence of crustal strength on rift geometry and development -insights from 3D numerical modelling. *Solid Earth* **14**, 369–388 (2023). https://doi.org/10.5194/se-14-369-2023

67. Pensa, T., Huertas, A. D. & Afifi, A. M. Desiccation of the Red Sea basin at the start of the Messinian salinity crisis was followed by major erosion and reflooding from the Indian Ocean. *Commun. Earth Environ.* **6**, 649 (2025). https://doi.org/10.1038/s43247-025-02642-1

68. Augustin, N. *et al.* 13 million years of seafloor spreading throughout the Red Sea Basin. *Nat. Commun.* **12**, 2427 (2021). https://doi.org/10.1038/s41467-021-22586-2

69. Shiddiqi, H. A. *et al.* Transform faulting in the Northern Red Sea revealed by ocean bottom seismometers deployed in the Zabargad Fracture Zone. *Geochem. Geophys. Geosyst.* **26**, e2025GC012253 (2025). https://doi.org/10.1029/2025GC012253

70. ElGabry, M. & Abdelazim, M. Seismicity of the Red Sea and Gulf of Aden. in *Seismotectonics of the East Mediterranean-Red Sea region* (eds. Hamimi, Z. et al.) 235–256 (Springer, 2025). https://doi.org/10.1007/978-3-031-80928-6_14

71. Mitchell, N. C., Izzeldin, A. Y. & Stewart, I. C. F. Nubia-Arabia separation: Clues from oceanic spreading fabric in the Red Sea. *Gondwana Res.* **147**, 301–320 (2025). https://doi.org/10.1016/j.gr.2025.06.019.

72. Hughes, G. W. & Johnson, R. S. Lithostratigraphy of the Red Sea region. *GeoArabia* **10**, 49–126 (2005). https://doi.org/10.2113/geoarabia100349

Acknowledgement

We thank Mr. Dia Mahmoud, GEOPEX Ltd. and Dr. Hussein Hammouda, Ex-Chairman of Egyptian Mineral Resources Authority, for their help in digitizing the old Red Sea magnetic and gravity paper sheets. Special thanks to the late Dr. Wafik Mishrif for his support and encouragement in collecting most of magnetic and gravity sheets over Gulf of Suez and Red Sea. Thanks to The National Geophysical Data Center (NGDC) for delivering the copy of gravity and magnetic data acquired over Red Sea. Thanks to Dr. Hans A. Roeser for providing his own gravity and magnetic material of 1975, 1976 and 1980.

Supplementary Information

The online version of this article includes a comprehensive Supplementary Information PDF comprising five figures (S1-S5) with detailed technical descriptions. These materials provide the empirical benchmarks, including regional gravity forward models, seismic refraction velocity data, and high-resolution multi-channel seismic reflection profiles, required to constrain the 12.5 Ma seafloor spreading model and verify the lateral dimensions of the interpreted magnetic domains.

Author contributions

KF: Conceptualization, Methodology, Data Acquisition, Formal Analysis, and Writing-Original Draft. AE: Data Curation, Writing-Review & Editing, and Technical Supervision.

Data availability

The regional geophysical datasets supporting the findings of this study are publicly available. Potential field and bathymetric data were integrated from the NOAA National Centers for Environmental Information (https://www.ngdc.noaa.gov), the UCSD Topographic/Bathymetric database (https://topex.ucsd.edu), and the

World Digital Magnetic Anomaly Map (WDMAM v2.1) repository (http://www.wdmam.org). Specific processed datasets or geospatial integrations generated during the current study are available from the corresponding author upon reasonable request.

Competing interests

The authors declare no competing interests.

Funding

No funding.

Figure Caption

Figure 1: Regional Geophysical and Geological Datasets of the Red Sea. Maps (a) and (b) present the regional gravity and magnetic intensity anomalies, respectively. Maps (c) and (d) illustrate the regional bathymetry. Map (e) provides a synthesized surface geological framework showing Precambrian suture zones (red lines) and crustal age domains/growth phases of the Arabian–Nubian Shield (Fritz et al., 2013). In map (c), yellow solid lines indicate the locations of VEMA seismic refraction profiles (sourced from NCEI), red boxes delineate previously studied geophysical focus areas and red circles identify the locations of hydrothermal brine deeps. In map (d), Cyan filled indicate bathymetric profiles along the axial trough and the blue lines are the published magnetic/gravity/seismic profiles modeling.

Data Sources: Potential field and bathymetric data were integrated from the World Digital Magnetic Anomaly Map (WDMAM v2.1), NOAA National Centers for Environmental Information (NCEI), and the UCSD Topographic/Bathymetric database. Map backgrounds are provided by Earthstar Geographics.

Figure 2: Regional 1900 km Seismic Refraction. (a) A synthesized and reconstructed crustal cross-section spanning 1900 km along the Red Sea axis, integrated from legacy seismic refraction data (Drake and Girdler, 1964; Tramontini and Davies, 1969; Cochran, 1983).

(b) Spatial distribution of the 1958 VEMA-Atlantis seismic refraction stations (indicated in black). The model distinguishes between two primary crustal velocity domains: Continental Basement, characterized by velocities of 5.5–6.4 km/s, and Oceanic/Intrusive, defined by higher velocities of 6.7–7.31 km/s. These velocities provide key support for identifying the boundaries of the three structural provinces proposed in this study.

Figure 3: Integrated Tectonic and Magnetic Fabric of the Red Sea. Maps (a-d) delineate the four primary structural trends:(a) N-S basement faults; (b) Inherited Suture trends; (c) Najd Shear System trends; and (d) the Aqaba-Dead Sea transform-related faults. Map (e) illustrates the Southern Red Sea axial ridge, characterized by a high-amplitude gravity anomaly (110 km width; 800 km strike length), which terminates abruptly at the Nakasib Suture Zone, marking a major crustal boundary. Map (f) highlights five distinct groups of linear magnetic stripes identified along the central and southern provinces. These white dashed elongated signatures are interpreted as Vine-Matthews stripes, representing organized seafloor spreading. Notably, these magnetic stripes are intersected and segmented by the interpreted strike-slip faults (derived from trends in maps d), demonstrating that tectonic of Precambrian infrastructure and transform tectonics directly control the lateral offset and fragmentation of the oceanic crust.

Figure 4: Geophysical benchmarks and crustal validation models of Central Red Sea. All profiles have been regenerated from original sources to provide independent geometric and density benchmarks. (a) Regional gravity transect and 2D forward model (adapted from [20]), demonstrating that the central geophysical fit requires a high-density crustal core (3.0g/cm3) to match the observed gravity field over the axis. (b) Regional 2D gravity anomaly and lithospheric density (adapted from [38]); the broad +100 mGal anomaly reflects the complete replacement of lower-density continental basement (2.670g/cm3) by high-density mafic crust and anomalous underlapping mantle (3.250g/cm3). (c) 2D gravity model across the western margin (adapted from [46]), capturing the lateral progression from the stable continental shield to a dense oceanic-type basement beneath the Main Trough. (d) Multichannel seismic interpretation compiled across seven reflection profiles (adapted from [46]), where high-amplitude reflectors delineate a continuous oceanic domain extending laterally beyond the active axial zone.(e) Red Sea inset shows track locations: gravity profiles in blue, seismic lines in red. Arrow intervals mark the bounds of identified axial magnetic anomalies.

Figure 5: Spreading Evolution and Integrated Domain-Based Model. (a) Integration of regional geology and magnetic data featuring oceanization cells (black circles). Central Red Sea, a black arrow highlights a 64 km lateral offset of the northern sub-zone relative to the southern sub-zone at the Atlantis II Deep and Heya-Jeddah Terrane, The location of seismic refraction line 180-181 is indicated in map (a), confirming an oceanic origin with high crustal velocities (6.97 km/s) at the eastern end of profile A-A'. (b) Delineation of newly identified ancient oceanic crust in the Central Red Sea, constrained by the landward projections of the Nakasib from south and Sol Hamid-Alaqi Suture Plateaus from north (black dashed lines). where seismic profiles 1 to 27, see figure 4 for locations, illustrate an 80 km lateral extension of axial oceanic crust, terminating at near the continental margins. Also, 2D gravity modeling, see figure 4 for locations, showing a high-density crustal block (3 g/cm3) replacing the continental lithosphere (2.7g/cm3), (c) Synthesis of the final integrated crustal model. (d) The original 5 Ma spreading model [14]. (e) Magnetic profile A-A' (location in map b) traversing newly interpreted elongated magnetic stripes (white dashed lines). Based on the 1 cm/yr spreading rate [14,46], profile A-A' reveals at least 12.5 Ma of spreading history beneath the Miocene S-reflector. The magnetic polarity timescale in (e) follows the Geological Society of America (2022).

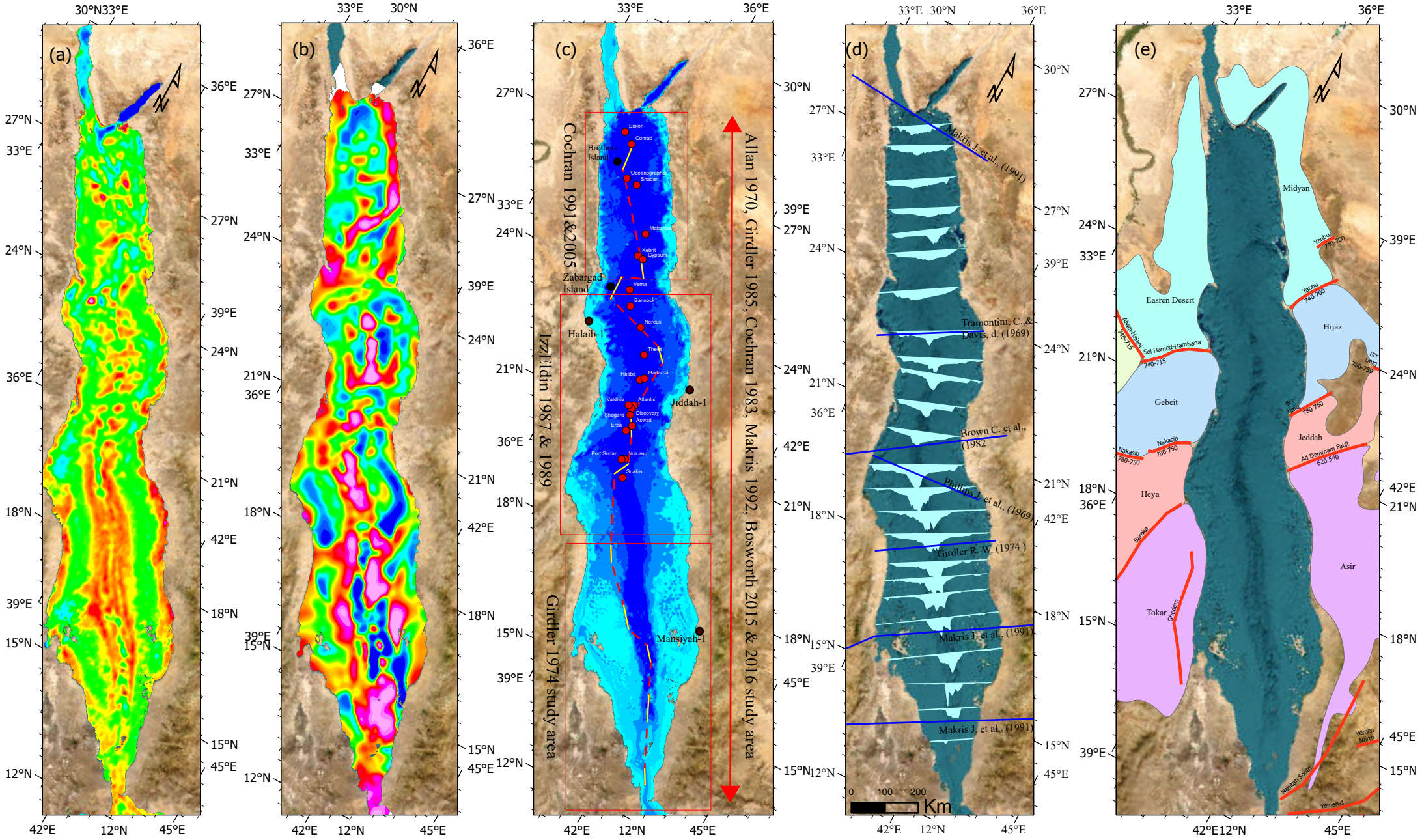

Figure 1: Regional Geophysical and Geological Datasets of the Red Sea. Maps (a) and (b) present the regional gravity and magnetic intensity anomalies, respectively. Maps (c) and (d) illustrate the regional bathymetry. Map (e) provides a synthesized surface geological framework showing Precambrian suture zones (red lines) and crustal age domains/growth phases of the Arabian–Nubian Shield (Fritz et al., 2013). In map (c), yellow solid lines indicate the locations of VEMA seismic refraction profiles (sourced from NCEI), red boxes delineate previously studied geophysical focus areas and red circles identify the locations of hydrothermal brine deeps. In map (d), Cyan filled profiles indicate bathymetric profiles along the axial trough and the blue lines are the published magnetic/gravity/seismic profiles with authors.

Data Sources: Potential field and bathymetric data were integrated from the World Digital Magnetic Anomaly Map (WDMAM v2.1), NOAA National Centers for Environmental Information (NCEI), and the UCSD Topographic/Bathymetric database. Map backgrounds are provided by Earthstar Geographics.

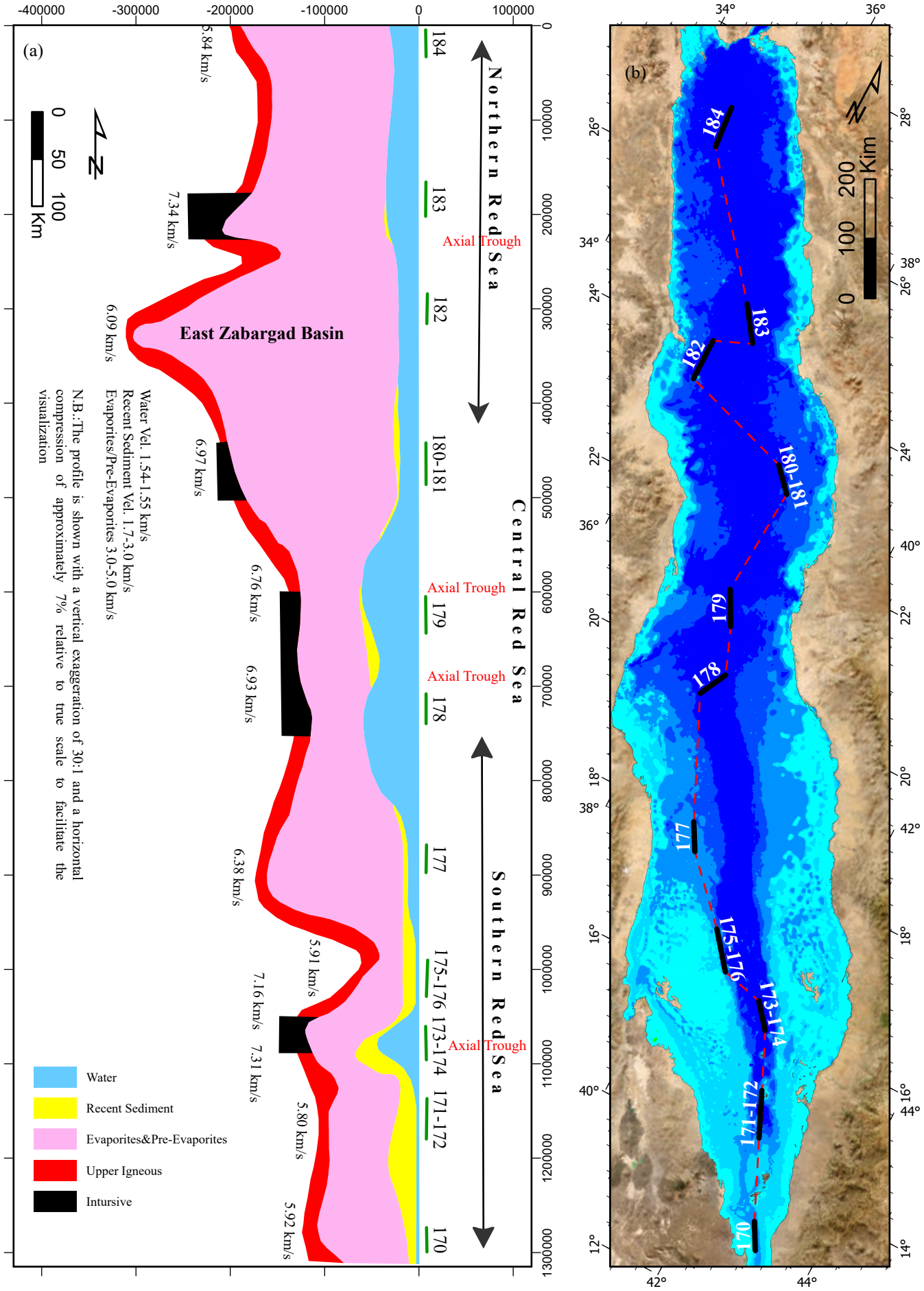

Figure 2: Regional 1900 km Seismic Refraction. (a) A synthesized and reconstructed crustal cross-section spanning 1900 km along the Red Sea axis, integrated from legacy seismic refraction data (Drake and Girdler, 1964; Tramontini and Davies, 1969; Cochran, 1983).
(b) Spatial distribution of the 1958 VEMA-Atlantis seismic refraction stations (indicated in black). The model distinguishes between two primary crustal velocity domains: Continental Basement, characterized by velocities of 5.5–6.4 km/s, and Oceanic/Intrusive Architecture, defined by higher velocities of 6.7–7.31 km/s. These velocity provide key support for identifying the boundaries of the three structural provinces proposed in this study.

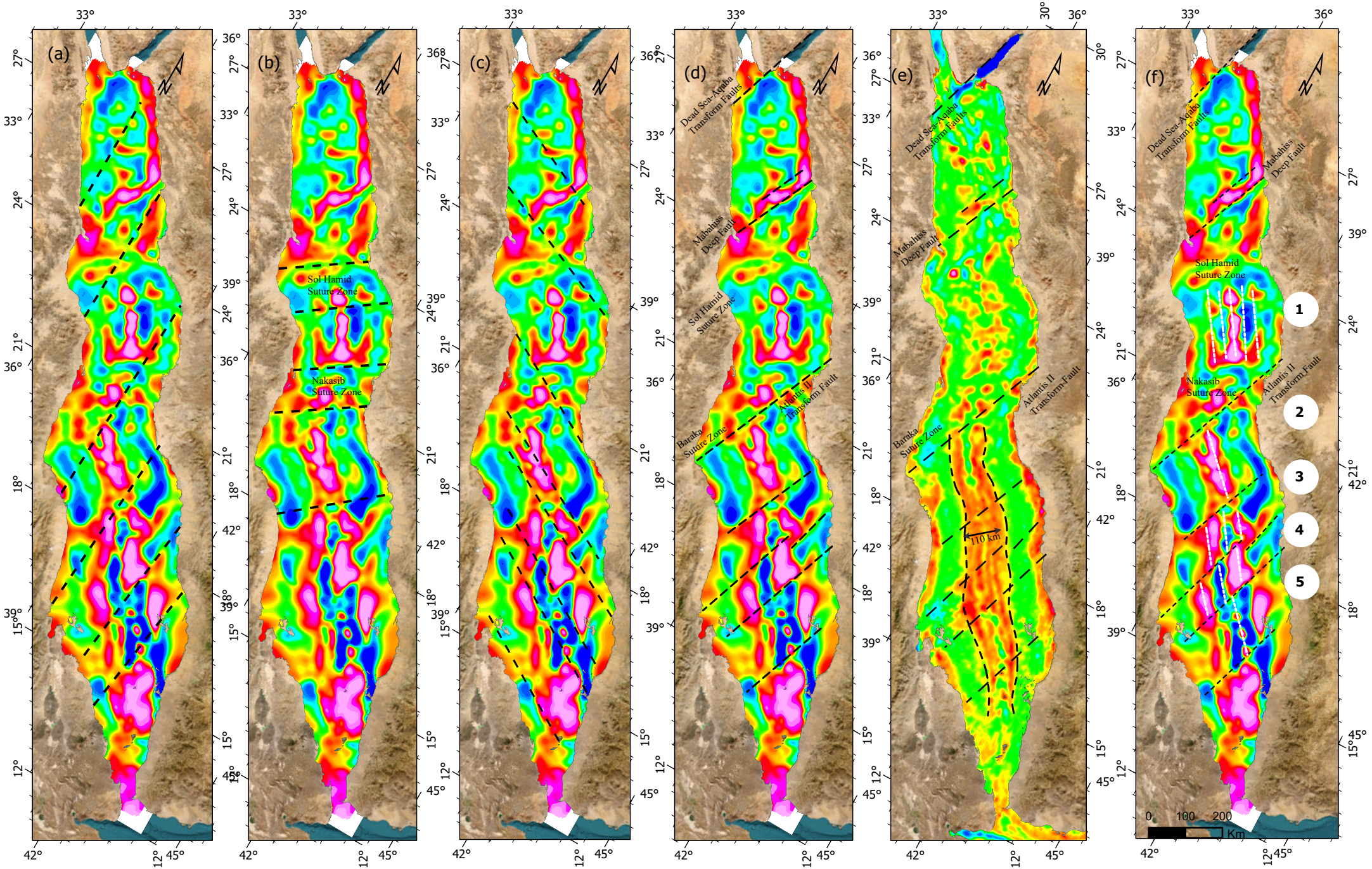

Figure 3: Integrated Tectonic and Magnetic Fabric of the Red Sea. Maps (a-d) delineate the four primary structural trends:(a) N-S basement faults; (b) Inherited Precambrian Suture trends; (c) Najd Shear System trends; and (d) the Aqaba-Dead Sea transform-related faults. Map (e) illustrates the Southern Red Sea axial ridge, characterized by a high-amplitude gravity anomaly (110 km width; 800 km strike length), which terminates abruptly at the Nakasib Suture Zone, marking a major crustal boundary. Map (f) highlights five distinct groups of linear magnetic stripes identified along the central and southern provinces. These white dashed elongated signatures are interpreted as Vine-Matthews stripes, representing organized seafloor spreading. Notably, these magnetic stripes are intersected and segmented by the interpreted strike-slip faults (derived from trends in maps d), demonstrating that inherited Precambrian infrastructure and transform tectonics directly control the lateral offset and fragmentation of the oceanic crust.

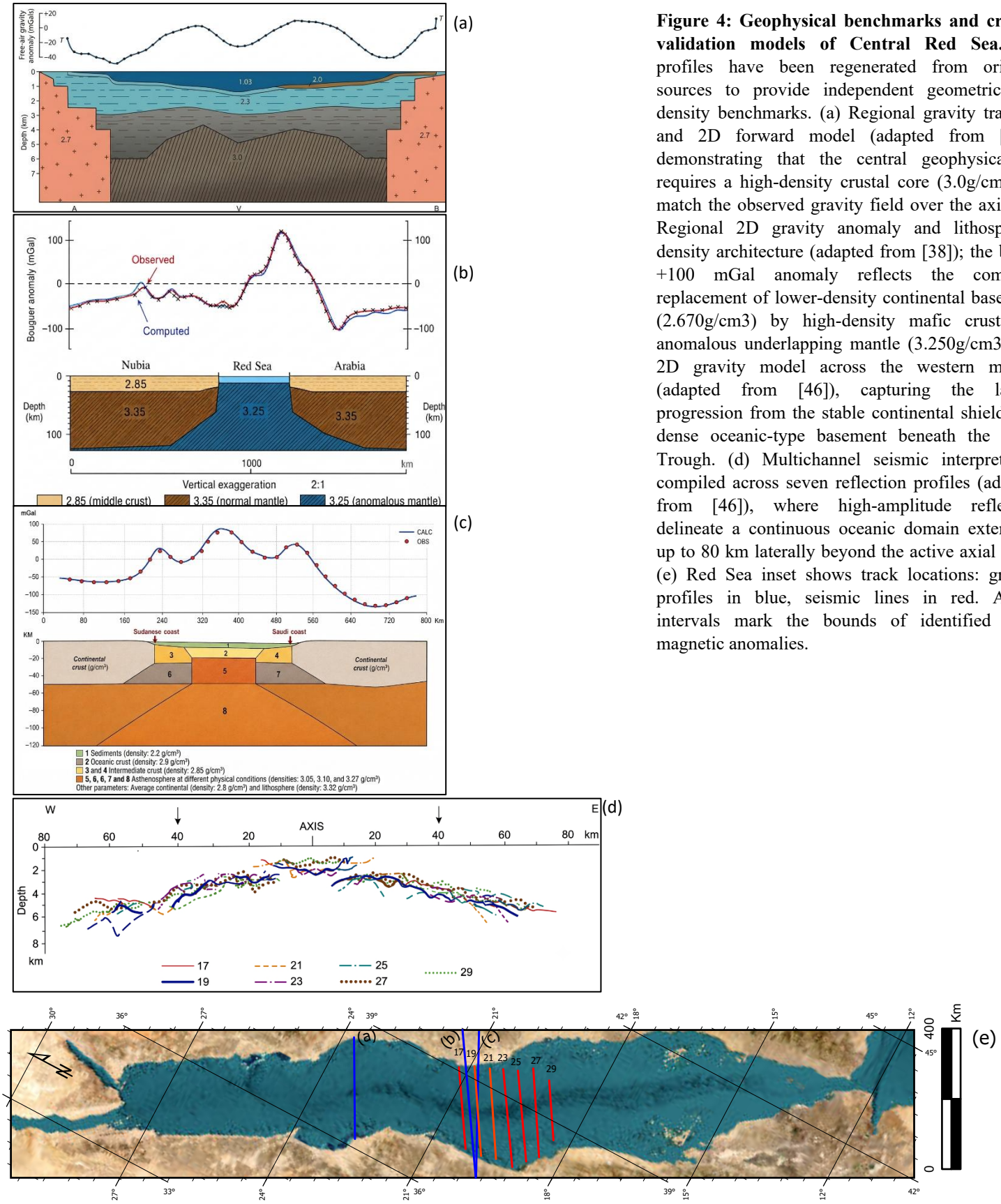

Figure 4: Geophysical benchmarks and crustal validation models of Central Red Sea. All profiles have been regenerated from original sources to provide independent geometric and density benchmarks. (a) Regional gravity transect and 2D forward model (adapted from [20]), demonstrating that the central geophysical fit requires a high-density crustal core (3.0g/cm3) to match the observed gravity field over the axis. (b) Regional 2D gravity anomaly and lithospheric density architecture (adapted from [38]); the broad +100 mGal anomaly reflects the complete replacement of lower-density continental basement (2.670g/cm3) by high-density mafic crust and anomalous underlapping mantle (3.250g/cm3). (c) 2D gravity model across the western margin (adapted from [46]), capturing the lateral progression from the stable continental shield to a dense oceanic-type basement beneath the Main Trough. (d) Multichannel seismic interpretation compiled across seven reflection profiles (adapted from [46]), where high-amplitude reflectors delineate a continuous oceanic domain extending up to 80 km laterally beyond the active axial zone. (e) Red Sea inset shows track locations: gravity profiles in blue, seismic lines in red. Arrow intervals mark the bounds of identified axial magnetic anomalies.

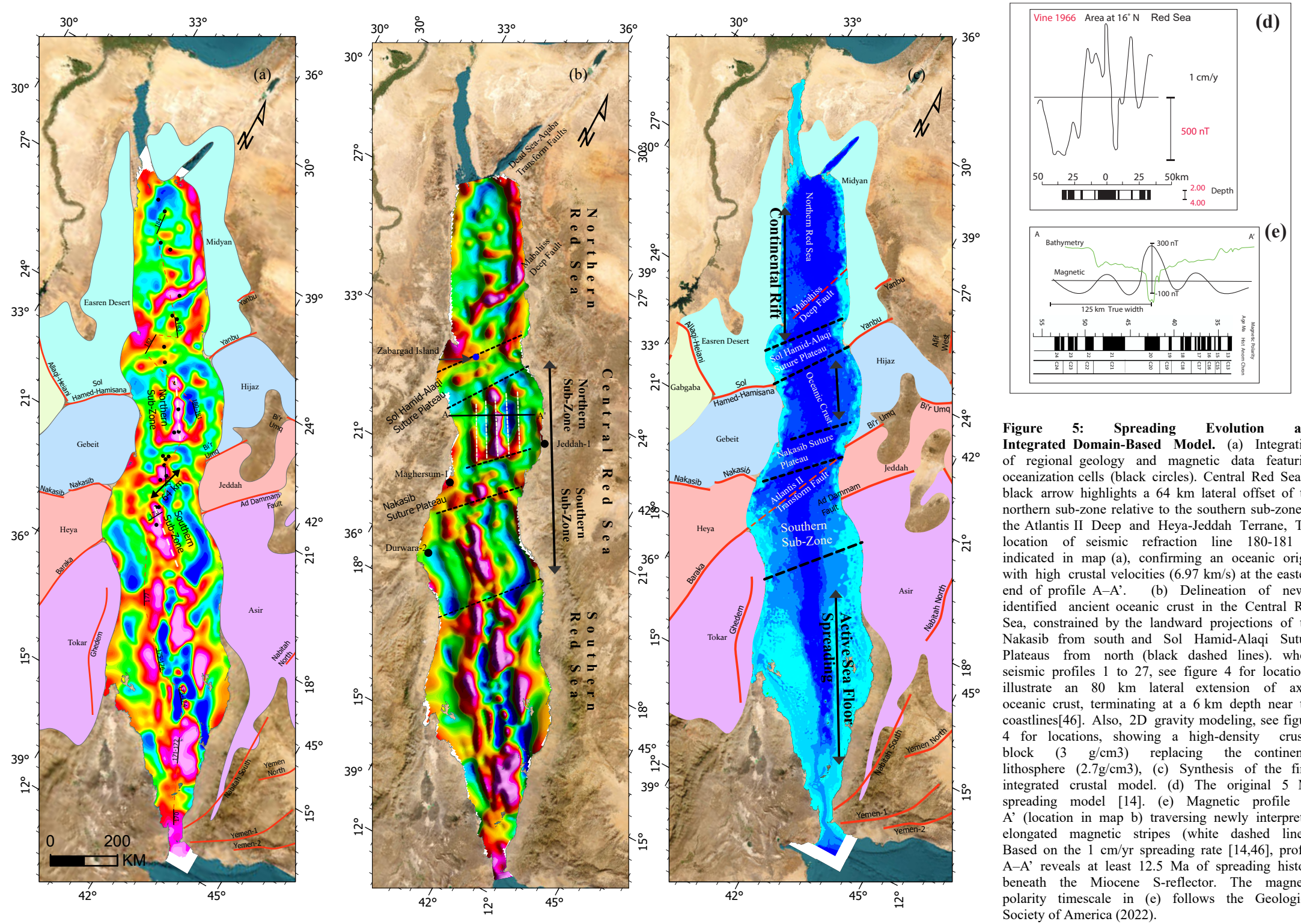

Figure 5: Spreading Evolution and Integrated Domain-Based Model. (a) Integration of regional geology and magnetic data featuring oceanization cells (black circles). Central Red Sea, a black arrow highlights a 64 km lateral offset of the northern sub-zone relative to the southern sub-zone at the Atlantis II Deep and Heya-Jeddah Terrane, The location of seismic refraction line 180-181 is indicated in map (a), confirming an oceanic origin with high crustal velocities (6.97 km/s) at the eastern end of profile A–A'. (b) Delineation of newly identified ancient oceanic crust in the Central Red Sea, constrained by the landward projections of the Nakasib from south and Sol Hamid-Alaqi Suture Plateaus from north (black dashed lines). where seismic profiles 1 to 27, see figure 4 for locations, illustrate an 80 km lateral extension of axial oceanic crust, terminating at a 6 km depth near the coastlines[46]. Also, 2D gravity modeling, see figure 4 for locations, showing a high-density crustal block (3 g/cm3) replacing the continental lithosphere (2.7g/cm3), (c) Synthesis of the final integrated crustal model. (d) The original 5 Ma spreading model [14]. (e) Magnetic profile A-A' (location in map b) traversing newly interpreted elongated magnetic stripes (white dashed lines). Based on the 1 cm/yr spreading rate [14,46], profile A–A' reveals at least 12.5 Ma of spreading history beneath the Miocene S-reflector. The magnetic polarity timescale in (e) follows the Geological Society of America (2022).